CMAC Smallsat Atmospheric Correction with Scene Statistics: Superior Accuracy in Near Real-Time

David Groeneveld and Tim Ruggles
Advanced Remote Sensing, Inc.
Sioux Falls South Dakota; (505) 690-6864
david@advancedremotesensing.com

ABSTRACT

The future of remote sensing is imaging smallsats; however, assuring their data utility requires atmospheric correction (AC). Current methods are difficult to apply and often fail to provide accurate surface reflectance retrieval even for the most common levels of atmospheric aerosol loading; this impediment is increasing annually due to wildfires induced by climate change. Closed-form Method for Atmospheric Correction (CMAC), developed for smallsats using Sentinel-2 data, is applicable to all imaging satellites. CMAC uses only scene statistics for automated near real-time AC while bypassing ancillary data that delays existing methods by days. In this paper, data from two research-grade satellite systems, Landsat-8/9 and Sentinel-2, were test corrected by CMAC for 323 individual image/area-of-interest combinations and compared to two bespoke industry-accepted software packages, LaSRC and Sen2Cor. The CMAC Sentinel-2 calibration was adjusted to Landsat-8/9 spectral responses using single points per band as a test for rapid calibration of smallsats. The results verified CMAC accurately retrieved the same surface reflectance distribution as LaSRC, but without limitations imposed through radiative transfer. CMAC-corrected data were more accurate than both Sen2Cor and LaSRC over a much wider range of atmospheric effect. These results are verifiable through cloud-based test-corrections and publicly available data-analysis spreadsheets.

1. INTRODUCTION

All atmospheric correction (AC) methods currently in use are based upon radiative transfer (RadTran) [1]. Though a logical theoretic approach, RadTran is an impediment for smallsats because the radiance responses of the sensors must first be known for application. These responses are well known to change after launch and during orbit [2], hence requiring periodic recalibration to assure accurate output of top-of-atmosphere reflectance (TOAR). Closed-form Method for Atmospheric Correction (CMAC) was developed specifically to overcome such RadTran limitations in service to the smallsat industry.

Large research-grade imaging systems such as Landsat 8/9 OLI (L8/9) and Sentinel 2A and 2B MSI (S2) are outfitted with on-board equipment to measure each band's radiance response so that adjustments can be calculated to deliver accurate TOAR. Reflectance, not radiance, is the metric of interest for virtually all optical Earth observation. The challenge for smallsat image utility is that the size and weight restrictions for economical launch force the omission of onboard calibration equipment to adjust for the variable and gradually changing sensor radiance responses.

The limitations imposed from unknown sensor radiance prompted development of a workaround that applies "harmonized" data [3], whereby each smallsat is periodically cross-calibrated to a satellite with known bandwise radiance such as L8/9 and S2. This process is problematic for several reasons: (1) inconvenience, since such cross calibration must be repeated periodically; (2) limited, because the availability of simultaneous overpasses is often problematic; and (3) contributing uncertainty due to differing relative spectral responses of the L8/9 and S2 sensors (Figure 1). However, a more severe problem is induced by atmospheric changes that occur during the period between overpasses, even across relatively short timespans (Figure 2). This timing problem can be regarded as a serious impediment for smallsats whose sun-synchronous overpasses occur well before or after the late morning overpasses by L8/9 and S2. This limits an application of primary interest for smallsat intelligence, surveillance, and reconnaissance (ISR) missions: keeping eyes on hotspots throughout the day, limited only by thick cloud cover.

CMAC was developed to offer atmospheric correction (AC) without the inherent problems of RadTran. A first goal was to make CMAC work in near real-time upon image download rather than waiting for a day or more to retrieve the additional data from a satellite (such as MODIS) [4] required to run RadTran [5]. CMAC uses only scene statistics, so it can function immediately upon download, or potentially reside onboard the smallsat. and with a lag of only seconds, correct each line of the image data as it is acquired. This hypothetical zero latency CMAC edge application is

afforded by push broom scanner operations that scroll the images during acquisition.

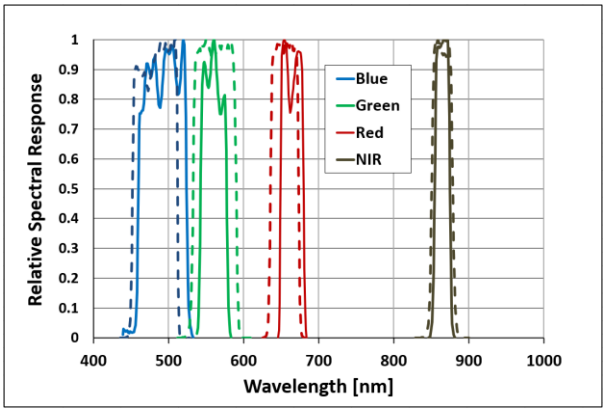

Figure 1. Relative spectral responses for Sentinel 2 (solid) and Landsat 8/9 (dashed).

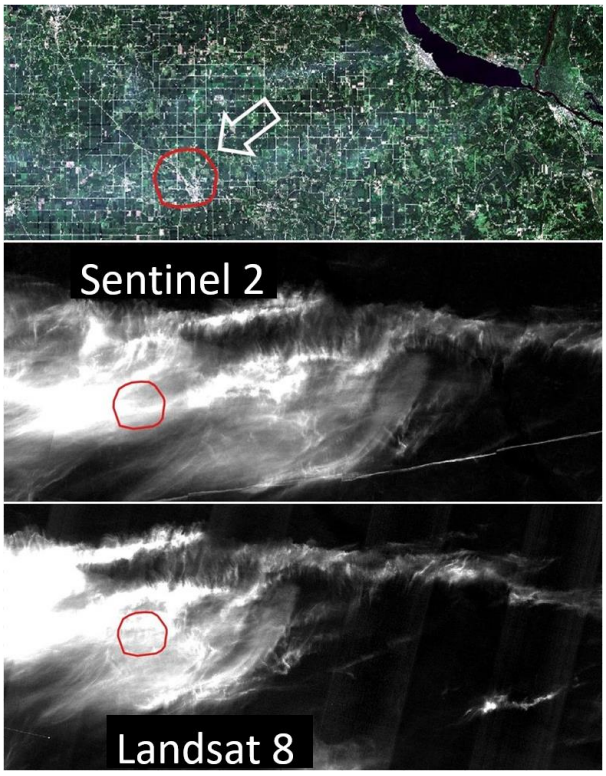

Figure 2. Cirrus can be seen in an RGB Sentinel 2 image. Inexact synchronicity is an error source in ancillary data; for example, the two cirrus band images were taken 18 minutes apart over central Minnesota. CMAC corrects cirrus band effects.

Real-time edge AC is made possible by CMAC because it is comparatively simple and applies closed-form mathematics that can correct an image to then be transmitted with only several seconds delay in critical path ISR, for example supporting active warfighting. Presently, the only option may be to accept uncorrected data with features variably obscured by haze rather than wait the extra time to receive and process an image. Delayed intelligence quickly loses value and with so many images being generated daily by smallsats (expected to soon be hundreds of thousands) will completely overwhelm the pool of human analysts. Automated AC that prepares images for AI workflows is the clear path forward for smallsat ISR.

Application of artificial intelligence for feature extraction (e.g., troop concentrations, artillery, tanks, etc.) is best applied with atmospheric noise removed from the data. Beyond national security, such cleaned data serves virtually all image applications, including precision agriculture, hence is highly desired by users. This is especially important now, when climate change induced wildfires are severely decreasing the percentage of clear days. The imaging smallsat industry is growing and while image supply may currently exceed demand, the time is at hand when image quality and timeliness will become the deciding factors to choose one image vendor over another.

Application of AC requires some degree of calibration, an example being data harmonization. CMAC also requires calibration for each sensor; however, this application is simpler and relatively easily applied because it uses reflectance to bypass sensor radiometry. By assuming pre-launch radiance calibration, the assumed TOAR can be calculated following the well-known convention for image processing workflow [6]. The step of calibrating the smallsat for the CMAC algorithm adjusts two parameters for conversion from the assumed TOAR to surface reflectance, as explained in the Methods section. The calibration procedure automatically accommodates differences from actual TOAR versus the assumed TOAR for retrieval of surface reflectance. Once these two parameters are calibrated for a smallsat, its data can be converted to surface reflectance for any location from then on, though subject to periodic recalibration to account for changes in sensor output. The calibration procedure is rapid and will be automated for each smallsat using data acquired through a purpose-built, monitored calibration target.

This paper presents a short recap of CMAC specific to smallsat applications; the interested reader can download a more detailed open source description and access live spreadsheets of statistical analyses, generic Python CMAC code, and a link for a cloud-based application to make test corrections of S2 data with features to browse and select images [7]. S2 data have served as the chosen testbed for CMAC development because: (1) they are supplied free of charge; (2) have relatively rapid cadence ($\geq$ 1 every 5 days); (3) are of excellent quality; and (4) have optimal resolution for

R&D. Translation of CMAC from S2 to smallsats or other sensors can be readily made; however, it should be noted that higher resolution enhances the granularity for assessing atmospheric effects while reducing the confounding influence of spectral mixing. With the evolutionary trend for increasing smallsat resolution, CMAC's AC performance will be enhanced.

2. METHODS

CMAC corrects imagery for a calibrated sensor in two processing steps. The first step maps atmospheric effects across the image as a grayscale. The second step then uses this map as the sole input to adjust the magnitude of the correction in each band, reversing the atmospheric effects to retrieve rasters of surface reflectance. As indicated earlier, each band requires calibration in a process that is rapid and precise. The description of CMAC development and operation provided in Groeneveld et al. [7] provides more detail.

2.1 Scaling Images for Atmospheric Correction

The first CMAC R&D effort was undertaken to develop a lumped-sum index of atmospheric effects directly from TOAR images. This workflow focused on the spectra of continuous healthy plant canopies that are described in the literature as dense dark vegetation (DDV) [8]. Using an ASD field spectrometer, potential target reflectances typical of DDV canopies were identified as a reference for assessing atmospherically induced changes from surface reflectance. DDV spectra are remarkably similar and stable in blue wavelengths. Healthy plants growing exposed to the open sky absorb nearly all blue light for photosynthesis to enable growth in partial shade. These plants deal with the solar energy in clear midday conditions by dissipating it as heat [9]. This process is mediated by carotenoid pigments [10] that reflect in the yellow-orange spectrum and absorb the blue light residual from photosynthesis. Because of this stability, the S2 blue band (B02) was, chosen as the basis for an atmospheric index.

To test the concept to use DDV surface reflectance, the lowest non-water blue band values discriminated in non-overlapping grid cells arrayed across images dominated by DDV were examine in images of the Amazon Basin and intensive mechanized farming of the American Midwest. This step confirmed that a workflow employing vegetation as a surface reflectance reference can produce highly sensitive grayscale maps that emulate visible haze. However, this application alone would be limited only to areas with sufficient DDV. This was solved using the blue band response for DDV of crops commonly grown under both irrigated and rainfed conditions to model atmospheric effects from nearby sampled areas supporting no vegetation cover in deserts to the cropped fields of the Midwest. The blue reflectance of DDV was measured on this crop cover and used as the dependent variable that was statistically modeled using the spectral responses from a wide range of adjacent vegetation under clear to highly wildfire-smoke-affected skies. The resulting model enables use of band statistics to estimate an atmospheric index, Atm-I, from scene statistics alone, providing for CMAC correction scaled by grayscale brightness (Figure 3). The Atm-I index is calibrated to vegetation reflectance measured as TOAR x 10,000.

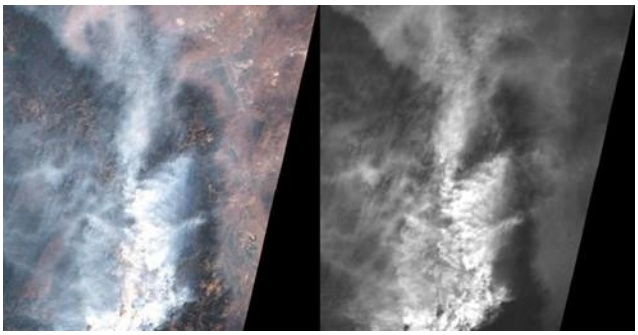

Figure 3. An example 100 m resolution (10 × 10 pixel grid cell) Atm-I grayscale for the 8-22-21 S2 tile over Lake Tahoe, CA, USA. At least some ground signal must remain for correction (exceeded in portions of this image).

2.2 Reversing TOAR to Surface Reflectance

CMAC mathematics applies observations of reflectance behavior that greatly simplify AC in comparison to RadTran. This approach began with observation of reflectance changes that occur due to atmospheric effects in every band: dark reflectance is brightened by backscatter while bright reflectance is darkened by attenuation. This response forms a continuum, hence, between positive (dark reflectance) and negative (bright reflectance) responses there exists a reflectance level where TOAR equals surface reflectance. This observation was translated into a graphic conceptual model (Figure 4) that inverts and adjusts the well-known empirical line method [11], resulting in a linear representation of the effect upon any pixel value from the overlying atmosphere at the time of image capture. This TOAR deviation line is uniquely defined by its slope and offset, which are the two parameters required for CMAC processing.

Precedence for the conceptual model and its linearity can be found in the literature reproduced as Figure 5 [12]. As Atm-I increases, both backscatter (defined by offset) increases, and attenuation (defined by both slope and offset) decreases the reflectance.

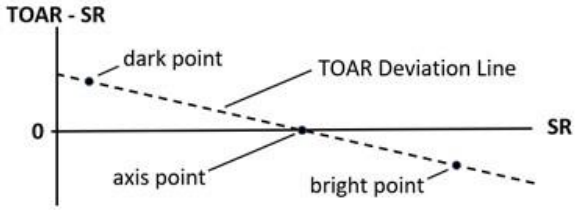

Figure 4. CMAC conceptual model expressing the effect upon dark to bright pixel values from any set level of atmospheric aerosol content. Slope and offset define the TOAR deviation line that crosses the x-axis at the axis point. SR is surface reflectance. Each TOAR deviation line is defined by a slope and an offset.

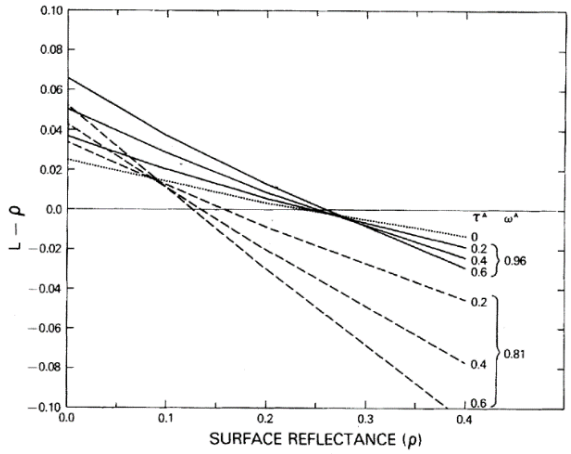

Figure 5. Figure 2 reproduced from Fraser and Kaufmann [12].

The conceptual model was further translated into the closed-form CMAC Equation allowing rapid correction of all pixels in an image guided only by the Atm-I grayscale. The mathematical relationships translating grayscale brightness into slope (m) and offset (b) parameters are developed through calibration.

CMAC Equation**:** $SR = (TOAR - b)/(m + 1)$

Though appropriate for initial visualization, the conceptual model and equation are not the complete solution for AC. An additional complexity arises from forward scatter effects that increase as the reflectance from the Earth's surface increases, thereby backlighting suspended particulates. Greater energy from brighter targets increases the degree of forward scatter. This does not affect the offset but does impact the slope by raising the bright point reflectance and migrating the axis point rightward as Atm-I increases (Figure 4). The effect upon smallsat calibration is to add an additional level of complexity for the use of calibration targets (Figure 6). As a promotional aspect, the combination of the effect of forward scatter through the Atm-I model provides a provisional method to remove spectral reflectance from water (Figure 7) requiring additional R&D to expand CMAC for reliable AC over oceans. RadTran cannot perform reliable AC over water despite keen interest for ISR application.

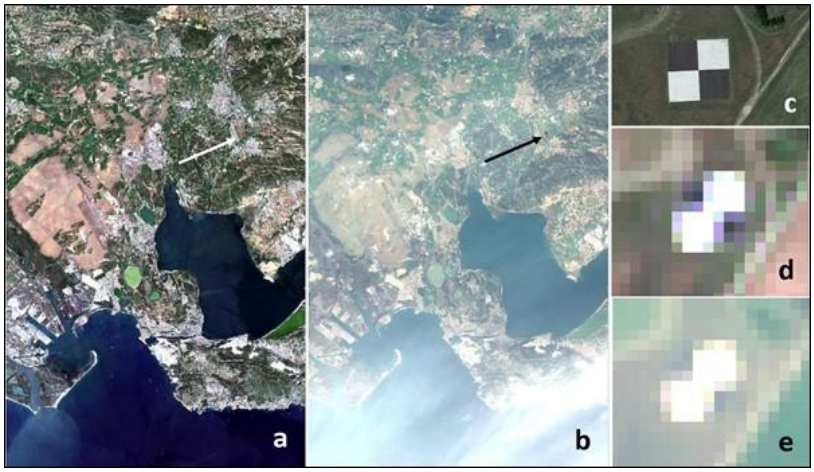

Figure 6. Salon de Provence, France region: a calibration target (arrows) in S2 TOAR regional images: 6-1-2021 under light haze (a, d) and 3-08-2021 under moderate haze from wildfire smoke (b, e). A Google Earth image (c) of the target shows the 30-m × 30-m black and white panels. Forward scatter is hypothesized to smear the bright targets while contracting the apparent dark targets. This effect may not be due solely to modulation transfer function issues.

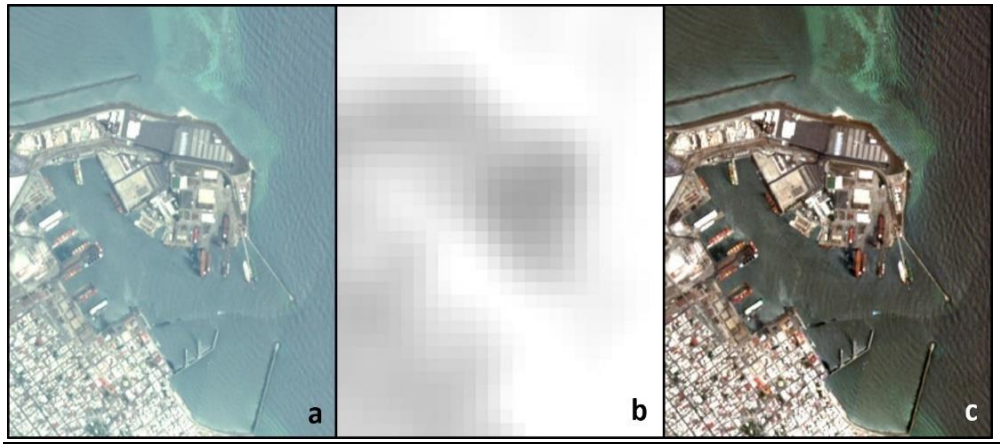

Figure 7. S2 image of Veracruz Harbor affected by smoke evenly mixed across the view: TOAR (a); Atm-I grayscale (b); and CMAC corrected (c). Atm-I over water is brighter due to specular reflectance. Cleared of this forward scatter, the CMAC view exposes benthic features (c).

2.3 Calibration for Translating the Atm-I Grayscale

Calibration for smallsats is best accomplished using calibration targets. However, as shown in Figure 6, the potential exists for degradation in the utility of a typical checkerboard target at higher Atm-I levels due to forward scatter. Such targets can best be reengineered by separating dark and bright panels, expanding the size of the dark panel, and addressing other concerns for drainage, security, cleaning accreted dust and achieving as Lambertian a surface as possible. In the interim, a combination of field measurements, image to image comparisons and reference to low Atm-I corrections by Sen2Cor created the present CMAC S2 calibration that delivered accurate surface reflectance estimation over a far wider window of atmospheric effects [7]. Calibration can apply areas of interest with invariant reflectance using images affected by varying degrees of Atm-I expression. Such quasi invariant areas (QIAs) are useful both for calibration and checking the statistics of AC output. QIAs used in these evaluations were warehouse-industrial districts for an area in Southern California (SoCal) east of Los Angeles (Figure 8).

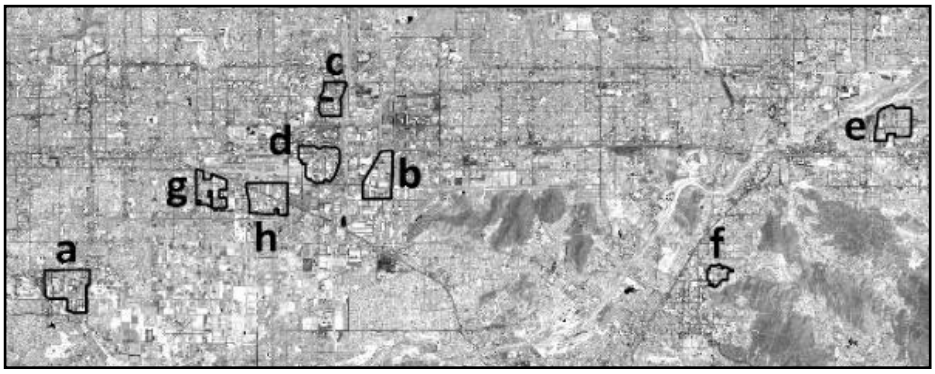

Figure 8. Eight QIAs supported CMAC testing that are named for their municipalities,: Chino (a); Fontana (b); Rochester (c); Ontario 1 (d); Redlands (e); Highgrove (f); Ontario 2 (g); and Ontario 3 (h).

2.4 Testing CMAC Against RadTran Methods

Testing for this paper included three treatments of reflectance – TOAR, CMAC and RadTran for the data of the four VNIR bands of S2 and L8/9 extracted from within the QIA boundaries. The images selected for analysis were restricted to the period from June 1 through August 15 to minimize solar zenith angle (SZA) variation from summer solstice. This restriction was made to control synergistic effects upon reflectance from variation in atmospheric pathlength through aerosol loading that increases with SZA. The cosine angle correction typically applied for S2 and L8/9 TOAR data is insufficient to account for the added effect from pathlength, hence, a bivariate correction is currently in preparation for CMAC.

Analysis A, Sentinel 2: Data were extracted from 28 images for the Chino, Fontana, Rochester, Ontario 1, Redlands and Highgrove QIAs. Prior to processing, images were vetted by visual inspection and discarded if clouds, including cirrus were present or if patchy not uniformly mixed haze existed for one or more QIAs. Atm-I was evaluated with a grid size of 60 by 60 pixels (i.e., 600 x 600 m) so that samples of dark reflectance from shadows, dark roofing, and vegetation were well represented in the sampled Atm-I.

Analysis B. Landsat 8/9: Data were extracted from 31 images of six of the eight QIAs (excluding Highgrove and Redlands) to concentrate analysis within the sidelap from adjacent tiles of L8/9: Chino, Fontana, Rochester, Ontario 1, Ontario 2, and Ontario 3. To accommodate the 30-m spatial resolution of L8/9, the applied Atm-I grid was adjusted to 20 x 20 pixels to scale the sampled areas as for Analysis A: 600 x 600 m.

The images chosen for these analyses capture the range of Atm-I most commonly encountered for routine image correction, from 800 to 1150. Ontario 1 data were not used in statistical analyses but were employed to test concepts for a rapid calibration procedure under development for smallsat application. This calibration was then applied to process the L8/9 data examined in this paper. This test calibration was generated from single points within each of the 4 VNIR bands, an effort requiring 6 person-hours to process, extract data and adjust the slopes and offsets of CMAC to match low Atm- LaSRC surface reflectance retrievals.

Prior CMAC R&D revealed that the value from individual estimates of surface reflectance is limited because mathematical context is lacking. The choice of QIAs with a range of reflectance values, low to high, provides reflectance distributions that convey a great deal more information than monotypic plots. For example, a single measured reflectance could be correct while the remaining distribution is wrong but not vice-versa. For developing an understanding of statistical distributions, CDFs were generated from reflectance

values measured at 22 percentile levels: increments of 0.1, 1, 3, 5 and 5 percentile to 95% were used for Analysis A. Analysis B omitted the 0.1% increment because the 30-m L8/9 spatial resolution limited statistical robustness for the lowest reflectance values.

Test-corrected images were compared as a qualitative indicator of the performance of the AC methods. Statistical testing for both analyses included average, standard deviation and coefficient of variation (CoV%) across the suite of images employed for each QIA. A logical, measurable fact for AC is that the clearest images (lowest Atm-I) provide "best available" estimates of true surface reflectance. Such best estimates were developed for each QIA of Analysis A and B: three of the 28 S2 images and five of the 31 L8/9 images were selected and averaged for each QIA. Multiple samples and averaging were made to control uncertainty. Best available estimates of surface reflectance were treated as the standard for percent error calculation of each percentile step of each image: % error = (value – standard)/standard x 100).

All numerical reflectance values in this paper were extracted from images and scaled by 10,000 following the convention adopted by the Sentinel 2 program. In the figures that follow, data are treated as DN (digital numbers) denoting that values were scaled to 16-bit unsigned integers. Spreadsheets supporting the statistical analysis reported here are available upon request.

3. RESULTS

As mentioned earlier, CMAC can be applied to any optical satellite imaging system, whether a smallsat such as the many hundreds now in orbit, or a research grade system such as S2 or L8/9. Testing of the CMAC technology here employed S2 and L8/9 for four important benefits beyond the fact that these data are public domain and offer a cost savings: (1) S2 quality, cadence and resolution were promotional for CMAC R&D; (2) Sen2Cor and LaSRC serve as industry-accepted milestones to compare to CMAC performance; (3) L8/9 data permitted test migration of CMAC to a new satellite and characterization of the effects from downscaling 10-m to 30-m pixels; and especially; (4) L8/9 served as a testbed for a rapid calibration concepts for planned application to smallsats that will be guided by the S2 master calibration.

Analysis A applied the CMAC v1.1 calibration for correction of S2 images throughout. Results in [7] demonstrated that image appearance is a competent indicator of true surface reflectance if the AC result is clear of haze and has correct color balance. That finding has been promotional for CMAC R&D because visual inspection provides rapid feedback with specificity as to which bands are exhibiting problematic correction. Although the relative spectral responses of S2 and L8/9 VNIR bands are similar, they are not equivalent (Figure 1). Once generated, the provisional calibration of CMAC L8/9 developed from a single points per band provided a reasonable match with groundtruth data, and provided visible confirmation that the calibration would deliver estimates close to true surface reflectance (Figure 9). CMAC v1.1 for L8/9, designated v1.1-L, was used for Analysis B surface reflectance retrieval. Appendix A presents images corrected by the four software packages, Sen2Cor, CMAC v1.1 (for S2), LaSRC, and CMAC v1.1-L for comparison.

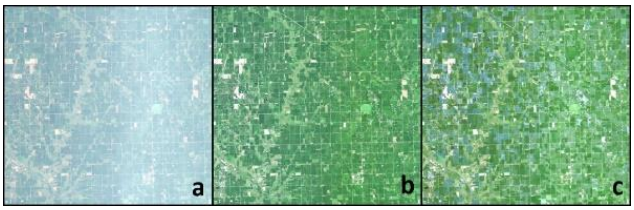

Figure 9. A view of the 8-11-18 L8 tile near Sioux Falls, SD affected by Canada wildfire smoke: (a) TOAR (b) corrected by CMAC; and (c) LaSRC with color balance issues.

3.1 Analysis A Results – Sentinel 2

The six Analysis A SoCal QIAs were evaluated by the same workflow. Table 1 provides a statistical summary for the grand averages of the 28 images across the QIAs for the three treatments: TOAR, CMAC and Sen2Cor. CV% is a measure of statistical dispersion: the greater the CV% magnitude, the more dispersed is the collection of values; hence, denoting lower precision.

A quick check through the CV% values confirms that CMAC performs well at the lower (dark) end of reflectance by having CV% values only slightly above those of TOAR. CMAC results in Table 1 show greater precision than Sen2Cor, especially for surface reflectance less than 2000 DN. This lower range of visible band reflectance carries the information sought by most remote sensing analyses; ready examples being the contrast/detail needed for AI feature extraction, measuring photosynthesis and biomass, assessing vegetation growth and yield, assessing productivity and ecologic health of water bodies, and especially as applied in CMAC, assessing Atm-I to scale AC. Other than from dry lake playas, salars, white sand beaches or ice/snow, high reflectance is generated primarily from artificial sources, e.g., from bright roofing. High surface reflectances are often masked from consideration during analyses and if otherwise of interest, can be readily identified using thresholds. The target of interest for AC of visible bands is reflectance less than about 2000 DN.

The Chino QIA is representative of the trends of the other five Analysis A QIAs. Average CDFs are presented in Figure 10 for the three treatments of the four bands of S2 data. CMAC and Sen2Cor show close agreement for reflectance below about 2000 DN. Discrepancies exist between CMAC and Sen2Cor output at higher reflectances; however, the 95% confidence interval for CMAC and Sen2Cor distributions overlapped through the entire range (data not shown). The question of which correction provided better accuracy is revisited in the Discussion section.

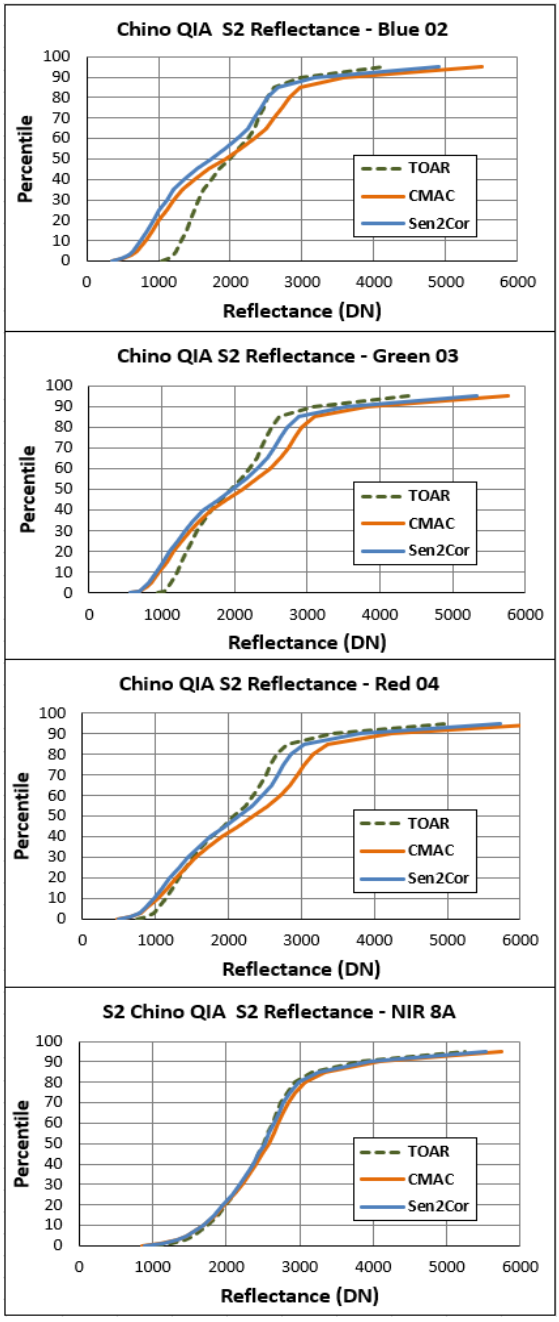

Figure 10. Average CDFs (n=28) of three treatments.

The grand-average CV% in Table 1 were calculated for each percentile across all six QIAs. Note that CV% and error from the QIAs can be pooled because they are derived values, while reflectance cannot since its distribution is dependent upon the collection of targets enclosed within each QIA boundary. The CV% for CMAC and Sen2Cor are close to the TOAR values but increase toward the high and low ends of the distributions. Of note are the more elevated values for darker Sen2Cor reflectance. Averaging the values from 28 images has masked the extreme values for the low end of the reflectance distribution, particularly for the blue band that requires the greatest degree of correction to retrieve surface reflectance.

Table 1. Grand average CV% for the distributions of the three treatments (6 SoCal QIAS; each point is 168 values). To save space, columns were shortened by eliminating even distribution steps, 50% or greater.

	Blue 02			Green 03			Red 04			NIR 8A		
%	TOAR	CMAC	S2C	TOAR	CMAC	S2C	TOAR	CMAC	S2C	TOAR	CMAC	S2C
0.1	5.5%	6.3%	23.6%	5.5%	6.0%	11.6%	7.0%	6.9%	11.5%	5.8%	6.2%	6.6%
1	4.7%	4.7%	16.0%	4.7%	5.1%	8.8%	5.6%	5.7%	8.2%	4.3%	4.6%	4.6%
3	4.2%	4.3%	12.4%	4.3%	4.7%	7.4%	4.9%	5.1%	6.8%	3.5%	3.8%	3.8%
5	3.9%	4.2%	10.9%	4.0%	4.5%	6.7%	4.5%	4.9%	6.1%	3.2%	3.6%	3.5%
10	3.6%	4.1%	8.9%	3.6%	4.4%	5.7%	4.0%	4.5%	5.1%	2.8%	3.2%	2.9%
15	3.3%	4.0%	7.6%	3.3%	4.2%	5.0%	3.5%	4.2%	4.4%	2.6%	3.0%	2.7%
20	3.0%	3.9%	6.6%	3.0%	3.9%	4.3%	3.1%	3.8%	3.7%	2.4%	2.9%	2.5%
25	2.8%	3.9%	5.9%	2.8%	3.8%	3.8%	2.8%	3.5%	3.2%	2.4%	2.8%	2.4%
30	2.6%	3.8%	5.1%	2.6%	3.7%	3.4%	2.6%	3.4%	2.9%	2.3%	2.8%	2.4%
35	2.4%	3.8%	4.5%	2.4%	3.6%	3.1%	2.4%	3.3%	2.7%	2.3%	2.8%	2.3%
40	2.3%	3.9%	4.0%	2.3%	3.6%	2.9%	2.4%	3.3%	2.6%	2.3%	2.7%	2.3%
45	2.3%	4.0%	3.6%	2.4%	3.7%	2.9%	2.4%	3.4%	2.6%	2.2%	2.7%	2.3%
55	2.4%	4.2%	3.4%	2.6%	3.9%	3.0%	2.6%	3.5%	2.7%	2.3%	2.7%	2.3%
65	2.9%	4.8%	3.9%	2.9%	4.2%	3.4%	2.7%	3.6%	2.9%	2.4%	2.8%	2.4%
75	3.2%	5.1%	4.3%	3.1%	4.3%	3.7%	3.0%	3.8%	3.2%	2.8%	3.3%	2.9%
85	4.7%	6.9%	6.2%	4.6%	6.0%	5.4%	4.8%	5.7%	5.2%	4.4%	4.9%	4.6%
95	5.8%	7.2%	6.9%	5.6%	6.4%	6.2%	5.5%	6.1%	5.8%	4.8%	5.2%	4.9%

The lower the Atm-I, the less correction is needed for the TOAR data; hence, as indicated earlier, corrected images affected by low Atm-I can be assumed to provide closer estimates of surface reflectance. Following this rationale and given that the reflectance distributions of the QIA's are stable, the reflectance data from CMAC and Sen2Cor distributions for the three lowest Atm-I images were averaged and used as the standard for calculation of an assumed percent error. The error estimates for the six QIAs were pooled, ranked and plotted for the four bands (Figure 11).

The striking high-magnitude, positive Sen2Cor errors in Figure 11 resulted from over estimation of surface reflectance near the dark ends of the reflectance distributions. These errors increase inversely with wavelength and contrast with CMAC error that shows little difference among bands (Figure 12). The ranked

error for CMAC is nearly equivalent for S2 correction (Figure 11) and L8/9 (provided later in Figure 14).

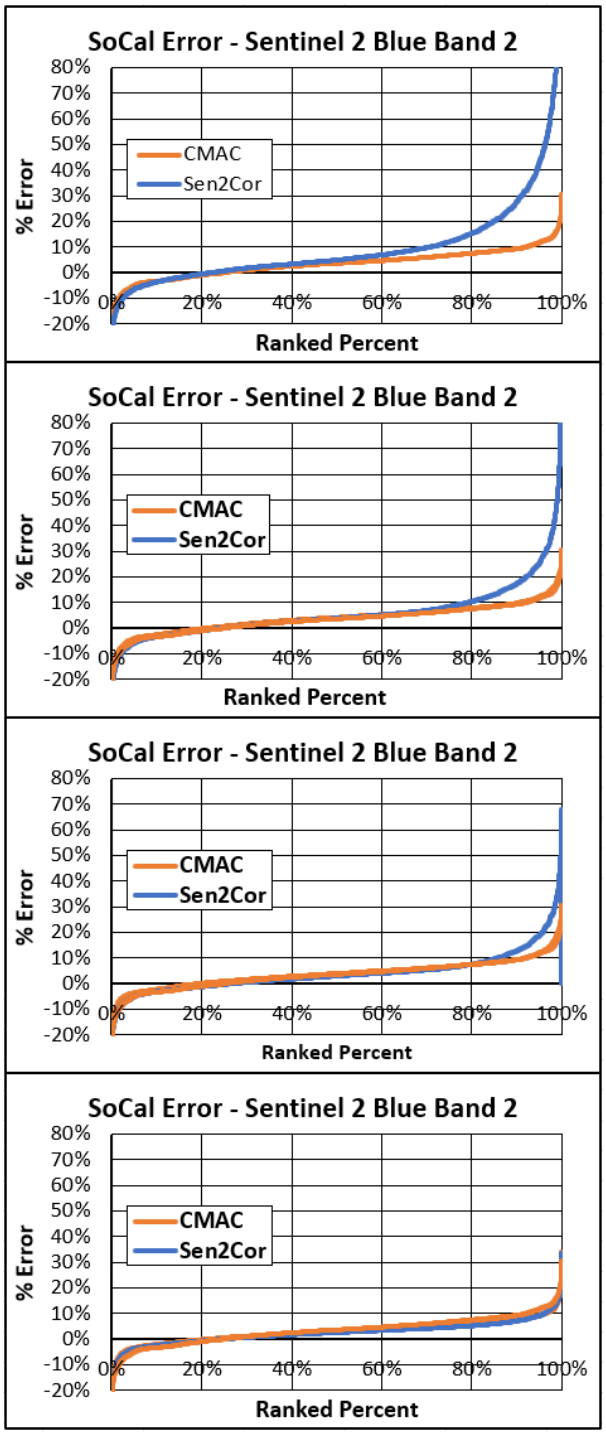

Figure 11. Error distributions for n = 3696 individual values (6 QIAs x 28 images x 22 percentiles) plotted for CMAC and Sen2Cor

Both CMAC and Sen2Cor distributions skewed several percent higher than expected – given the experimental design, the curves would be expected to cross the x-axis at the 50th percentile. A bias toward higher positive error is likely the result of systematic but slight under-correction as Atm-I increases. This small bias will be corrected in next-generation R&D that will finalize all CMAC relationships.

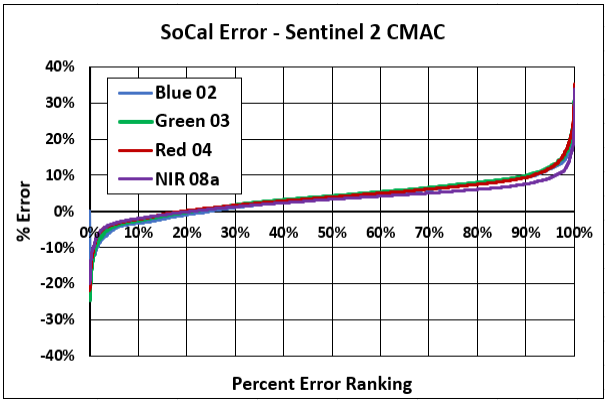

Figure 12. Sentinel 2 ranked % error plotted for CMAC.

To understand the range of Atm-I that can be corrected accurately by both methods, the low, dark end of reflectance was explored further since it is both highly important for data applications and where most of the estimation error was generated in these datasets. The absolute values of percent error were averaged across the 0.1, 1, 3, 5, 10, 15 and 20th percentiles of reflectance to form an error index, one value per image, that was plotted according to the recorded median image Atm-I. For all six QIAs, the % error values were combined, ranked and plotted (Figure 13). The reflectance range corresponding to the 20th percentile of the CDF encompasses up to 2000 DN for NIR 8a and about 1000 to 1200 DN for the visible bands in the Chino QIA example (Figure 10).

Regression lines are shown for the extracted data in the low reflectance scatter plots of Figure 13. These results show that Sen2Cor surface reflectance estimation for visible bands is accurate only at the lowest levels of atmospheric effect and accuracy decreases as Atm-I increases. The error for CMAC surface reflectance retrieval increases comparatively gradually with Atm-I and at a much lower rate than Sen2Cor. The trend that gave rise to the skewing in Figure 11 can be countered through further calibration work. Plots of error for low reflectance, as shown in Figure 13, provide the detail to better understand and counter overestimation error.

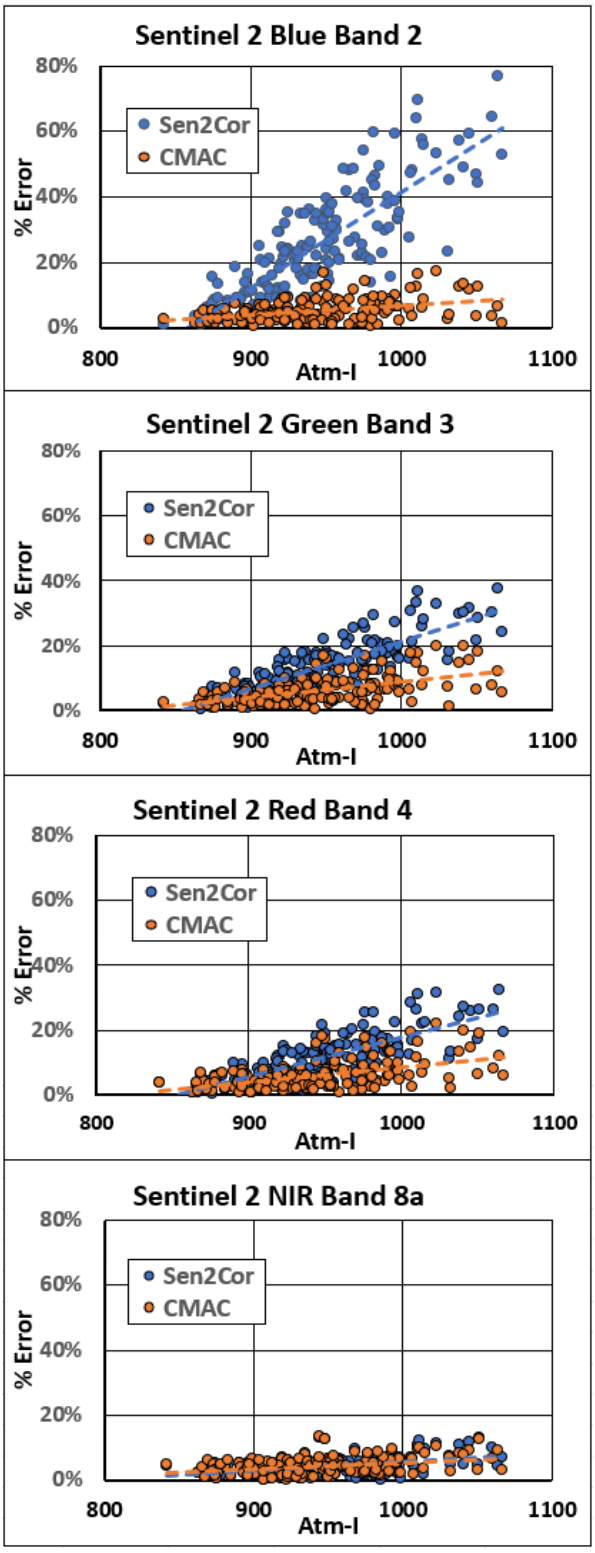

Figure 13. Estimated % error of low reflectance for the S2 SoCal data plotted according to the Atm-I level of the image (m=168; 6 QIAs x 22 percentiles). The Sen2Cor NIR regression line is hidden behind the CMAC regression line.

3.2 Analysis B Results – Landsat 8/9

Of the 31 images used for Analysis B, 24 are L8 images selected from 2019 through 2022 augmented by 7 images from L9 during 2022. The L8 and L9 images showed no discernable differences, thus their data were pooled for the analysis. Table 2 provides grand averages of the CV% for LaSRC AC across the five QIAs that resemble the same patterns seen for S2: greater dispersion for the lower limb of reflectance, especially in the blue band. Otherwise, there is relatively close agreement of CV% for the three treatments. Recall that the calibration producing the CMAC values is the result of using a single points per band that required six hours of effort. If atmospheric correction of L8/9 is of future interest, additional focus on calibration is expected to enhance CMAC correction, accuracy and precision.

Table 2. Average CV% as grand averages (n = 155) across the five QIAs. Even percentiles, 50-90%, were removed to save space.

	Blue 02			Green 03			Red 04			NIR 05		
%	TOAR	CMAC	LaSRC	TOAR	CMAC	LaSRC	TOAR	CMAC	LaSRC	TOAR	CMAC	LaSRC
1	5.7%	6.1%	26.7%	6.2%	5.9%	9.4%	6.6%	5.8%	8.5%	4.6%	5.2%	5.2%
3	5.3%	5.4%	13.7%	5.5%	5.0%	7.2%	5.7%	5.1%	6.5%	3.9%	3.9%	4.1%
5	5.0%	5.2%	10.0%	5.2%	4.7%	6.4%	5.2%	4.7%	5.8%	3.8%	3.3%	3.9%
10	4.6%	5.1%	6.7%	4.6%	4.5%	5.5%	4.5%	4.3%	4.8%	3.8%	3.1%	3.9%
15	4.2%	5.1%	5.5%	4.3%	4.5%	5.0%	4.1%	4.2%	4.3%	3.7%	3.1%	3.9%
20	4.0%	5.1%	4.7%	4.0%	4.5%	4.6%	3.9%	4.1%	4.0%	3.7%	3.2%	3.9%
25	3.9%	5.3%	4.4%	3.9%	4.6%	4.5%	3.8%	4.3%	3.9%	3.7%	3.2%	3.9%
30	3.7%	5.5%	4.3%	3.7%	4.7%	4.3%	3.6%	4.3%	3.8%	3.7%	3.3%	3.9%
35	3.6%	5.7%	4.2%	3.7%	4.8%	4.2%	3.6%	4.3%	3.7%	3.6%	3.3%	3.9%
40	3.6%	5.9%	4.2%	3.6%	4.9%	4.2%	3.5%	4.4%	3.7%	3.6%	3.3%	3.9%
45	3.6%	6.1%	4.3%	3.6%	5.1%	4.2%	3.5%	4.5%	3.8%	3.6%	3.4%	3.9%
55	3.7%	6.4%	4.6%	3.7%	5.3%	4.4%	3.7%	4.8%	4.0%	3.6%	3.5%	3.9%
65	4.0%	6.9%	4.9%	4.0%	5.7%	4.6%	3.8%	5.0%	4.1%	3.4%	3.5%	3.8%
75	4.2%	7.1%	5.3%	4.2%	5.8%	4.8%	4.0%	5.1%	4.3%	3.7%	4.0%	4.0%
85	5.1%	8.0%	7.4%	5.2%	6.7%	6.3%	5.4%	6.1%	6.0%	5.6%	6.1%	5.8%
95	7.6%	9.7%	9.6%	7.6%	8.3%	8.3%	7.6%	7.8%	7.9%	6.6%	6.8%	6.6%

Percent error was evaluated for L8/9 using the same methods as for S2: averages were applied as the closest-to-surface-reflectance standards for both CMAC and LaSRC determined from the five lowest Atm-I images in each band. The percent error calculated from the 31 images were combined, ranked from low to high, and plotted on Figure 14 that shows only minor discrepancies between the two methods. CMAC percent error distributions were lower for the S2 corrections in Figures 11 and 14.

Comparison of the overall error curves of Figures 11 with 14 discloses that LaSRC performs much better than Sen2Cor for surface reflectance retrieval. CMAC performed better than both these accepted methods, as indicated by its ranked error curves closer to the x axis which, in Cartesian space, represents zero error. CMAC also performed better than Sen2Cor and LaSRC for the low reflectance error plots in Figures 13 and 15.

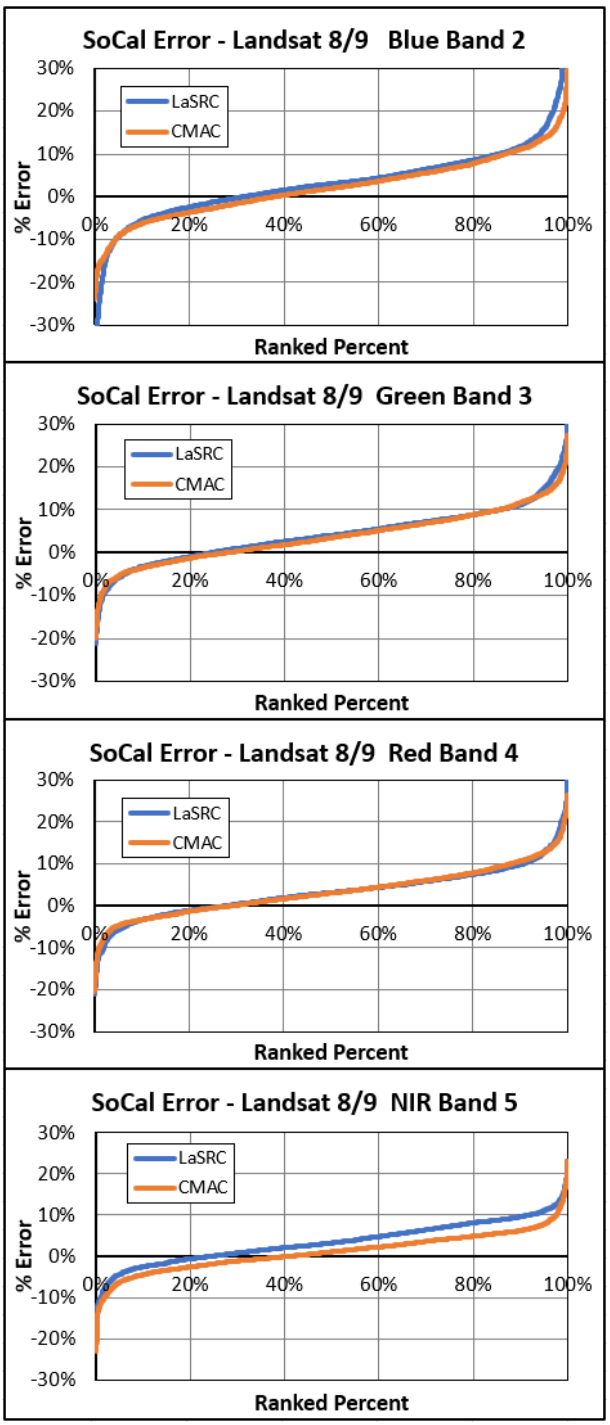

Figure 14. Error distribution for the four bands of CMAC and LaSRC are closer compared to CMAC and Sen2Cor (Figure 11).

As in the comparison of Sen2Cor and CMAC data in Section 3.1, the low surface reflectance estimates of L8/9 were subjected to error analysis calculated in the same manner: absolute values of percent error were averaged for the 1, 3, 5, 10, 15 and 20th percentiles to form a relative error index, one point per image. These index values were pooled and plotted according to the associated median Atm-I from the images. These data were pooled for the five Analysis B QIAs and plotted in Figure 15 according to Atm-I.

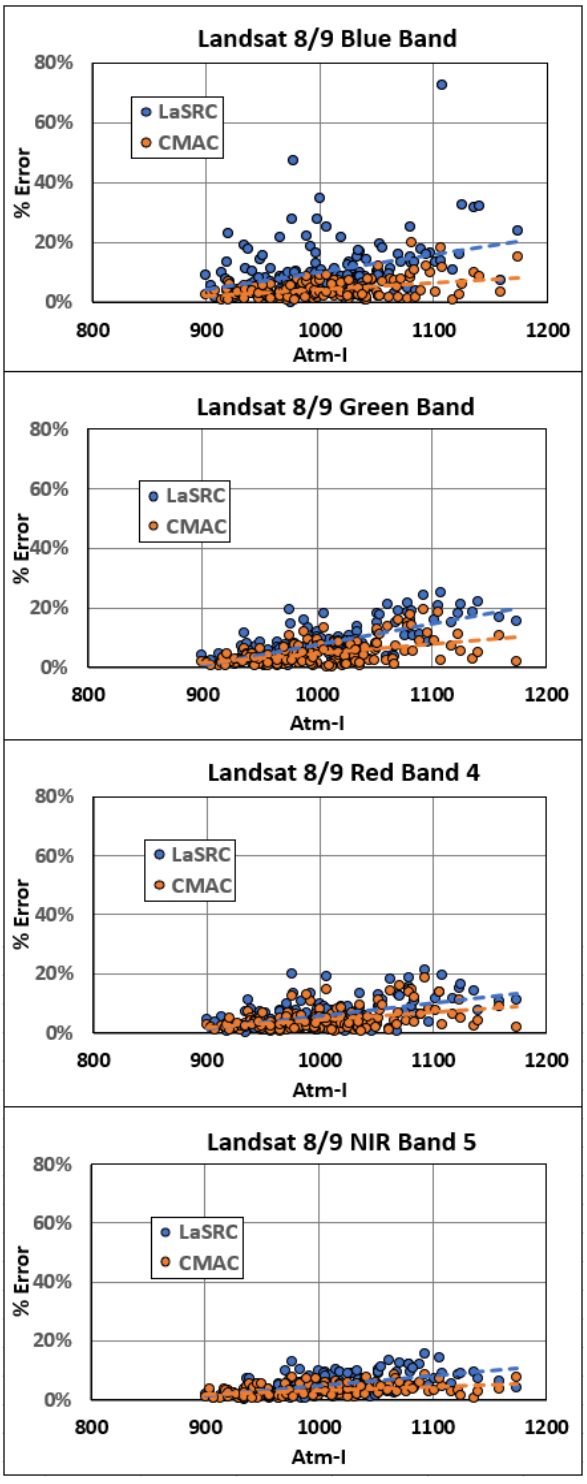

Figure 15. Average % error for low reflectance L8/9 data (n = 155)

As in Figure 13, regression lines were fitted for the low reflectance error indices of each band in Figure 15 and in all bands, the slopes of LaSRC exceeded CMAC results. The comparatively greater error in LaSRC agrees with results from the grand averages of CV% in Table 2, although the LaSRC errors were much lower in magnitude than for the Sen2Cor output of Figure 11. The CMAC visible-band error remained relatively constant across the 5-QIA dataset while error for LaSRC, slightly higher than CMAC for the red band, increased in the green band, and markedly increased in the blue band, similar to the results for Sen2Cor but to a lesser degree. For both Sen2Cor and LaSRC, increasing error toward the dark end of the visible-band reflectance distributions is problematic since this low end of reflectance conveys responses of greatest interest for virtually all uses as explained earlier.

CMAC error in the NIR band for both S2 (Figure 13) and L8/9 (Figure 15) data was well constrained across all levels of brightness as can be seen in the lower degree of scatter.

A final test for the L8/9 comparison was to examine the curves of bandwise TOAR and retrieved surface reflectance from CMAC and LaSRC. The data for each band and percentile step were averaged across the 31-image datasets for each QIA. The Chino QIA data, is presented in Figure 16. Comparison of the TOAR to the AC values shows a progressive decrease in the magnitude of the correction with increasing wavelength.

The Chino QIA results are roughly representative of the other four SoCal QIAs (data available upon request), showing virtually complete agreement for three bands, a result that held in most of the comparisons; for the Rochester QIA, all four bands were in similar agreement. The descrepancy between CMAC and LaSRC was greatest for all bands of all QIAs for the Chino blue band (Figure 16). For three of the five comparisons, the blue band showed very close agreement with the results from two of the QIAs, Ontario 3 and Rochester, showing nearly complete agreement.

The comparisons in Figure 16 are a check for whether the distribution shape and magnitude of the two methods agreed. Averaging across the large datasets of 31 images reduced uncertainty to enable accurate comparison of the two methods without allowing image by image variation to mask the result. The degree of such variation is also captured through the calculation of CV% displayed in Table 2. As mentioned in Section 2.4, the CMAC L8/9 calibration was modeled from the Ontario 1 low-Atm-I surface reflectance retrievals of LaSRC. Therefore, CMAC surface reflectance retrieval with high fidelity to LaSRC demonstrates that the CMAC conceptual model and its mathematical representation are a stable, reproducible and correct representation of atmospheric effcts upon transmitted light.

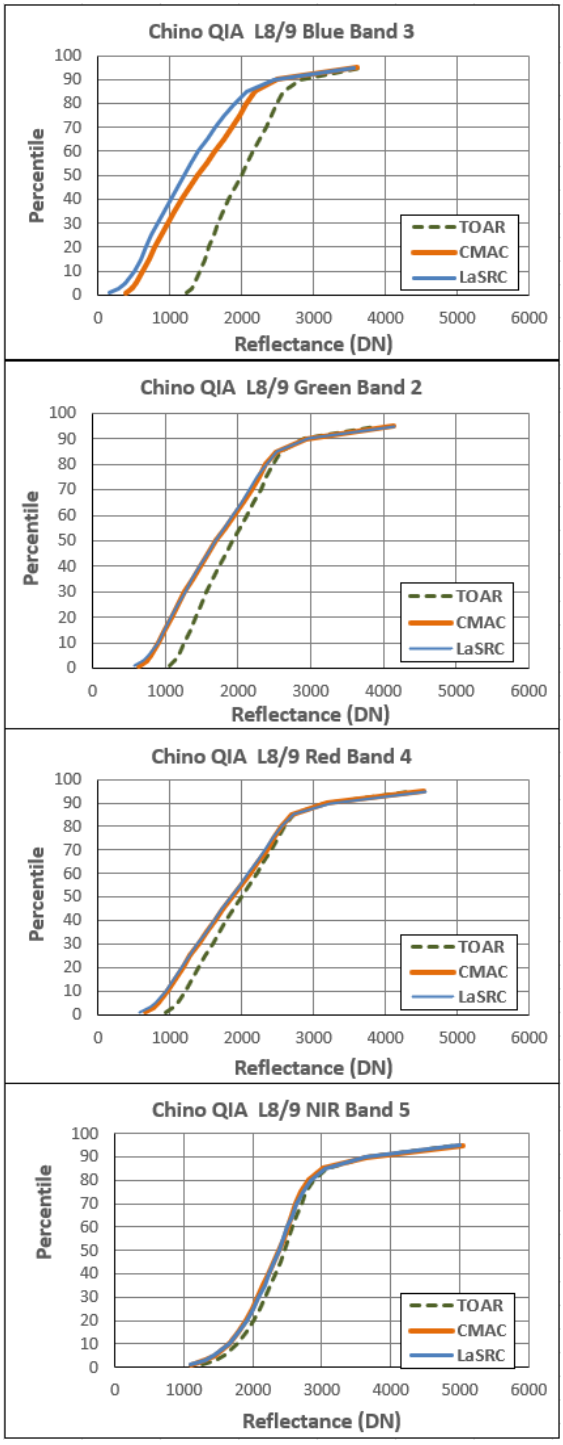

Figure 16. CMAC and LaSRC surface reflectance estimates compared to TOAR for the Chino QIA.

4. DISCUSSION

As previously mentioned, CMAC was created to serve the smallsat industry but is also appropriate for any imaging optical satellite. In extensive tests presented in this paper using S2 and L8/9 data, CMAC surface reflectance retrievals were compared with results from Sen2Cor and LaSRC software. Extensive examination of the appearance of corrected images and of the QIA statistics for surface reflectance retrievals confirmed that CMAC performed better than goth of these industry-accepted software packages. CMAC delivered accuracy and precision that surpassed Sen2Cor for all bands and for LaSRC at least in the blue band. Image processing for these analyses applied compiled C++ versions of CMAC that estimated surface reflectance using only scene statistics. Full tiles of S2 from this CMAC processing required, on average, 91 seconds and for full tiles of L8/9 about 60 seconds. This performance is near real-time in comparison to Sen2Cor and LaSRC, and without the further delay waiting for required ancillary data. Though CMAC performed well in these tests, it will be improved through ongoing R&D.

A particularly important finding was that the L8/9 CMAC version, initially calibrated by adjusting slope and offset parameters to match LaSRC response for the Ontario 1 QIA, retrieved surface reflectance of five other QIAs that closely match the average LaSRC surface reflectance retrievals with only one discrepancy in the blue band (Figure 16). The LaSRC blue band surface reflectance retrieval is less stable than the other three VNIR bands as shown through CV% (Table 2) and low reflectance error analysis (Figure 15). These results provide statistical verification that the CMAC conceptual model (Figure 4) and the CMAC equation translated from it, provided competent retrieval of surface reflectance that aligned nearly exactly with LaSRC's RadTran output while suffering none of its limitations. These and other conclusions can be confirmed through examination of spreadsheets that are available upon request.

The CMAC v1.1-L calibration was transferred from the S2 calibration version and used for AC of L8/9 data in this paper. The higher accuracy achieved here by CMAC supports provisional concepts for automated single-overpass calibration of unlimited numbers of smallsats.

A calibration target is required for complete automation of the calibration process for new smallsats. A target will provide highly precise inputs that will translate into greater accuracy and precision for smallsat surface reflectance retrieval. Except for employing a target, the same calibration concepts will follow the provisional workflow that established the L8 calibration for any new "proxy" smallsats by extrapolation of calibrated slope and offset relationships from a "master" sensor. For master-proxy calibration (MPC) presently, S2 serves as the master because of its higher spatial resolution, cadence and quality; however, any high quality satellite output could similarly be employed. MPC is a robust concept: hypothetically, all visible bands in the VNIR spectrum can be calibrated using MPC, even if no such band is measured by the master. Work is proceeding to confirm MPC for global application to all bands. If it works as hypothesized, it can be used to calibrate any VNIR band that is unaffected by variable atmospheric absorption, e.g., water vapor in portions of the NIR spectrum. Application of MPC to hyperspectral data may be a particularly fruitful application.

Next-generation R&D will upgrade the CMAC calibration program using nearly unlimited amounts of "groundtruth" gathered in a system employing non-imaging spectral acquisition through low-altitude hyperspectral flightlines (LHF) and accompanying GPS positioning and videography for each data point. Such systems take snapshots along the flightline that can then be paired with satellite data to enable calibration and development of mathematical relationships. This includes enhancing the precision of the CMAC realtionships and completion of a bivariate model to correct for the synergistic effect of SZA upon surface reflectance retrieval under varying levels of Atm-I. Another problem of particular interest is to develop methods for accurate verified retrieval of upwelling reflectance over water bodies including the ocean that factors in the role of specular reflectance from the water surface. Massive amounts of "groundtruth" will be necessary and can be generated rapidly through LHF. A piloted aircraft is better suited for this mission than drones that severely limit to/from travel for data collection, range and operation time, and flexibility for rapid adjustment for conditions.

An LHF system engineered to fly aboard a light aircraft can include 2 spectrometers, one uplooking to provide solar irradance to normalze the data to surface reflectance. An ideal system can be operated by a single pilot using an on-off switch. Such an LHF system proved valuable to support development of a satellite-based monitoring system in use now for a decade and a half [14, 15]. By selecting special conditions under which to gather groundtruth paired with TOAR satellite data, solutions can be developed for variable atmospheric conditions and ground targets. In combination, LHF and calibration targets are expected to produce rapid breakthroughs and finalize CMAC to

expand smallsat surface reflectance retrieval for all times of the day, for any environment and for any view, nadir to oblique at any azimuth.

CMAC technology is patented in the United States and patent pending in the United States and internationally.

5. REFERENCES

1. Zhang, H., D. Yan, B. Zhang, *Z.* Fu, B. Li, and S. Zhang, "An Operational Atmospheric Correction Framework for Multi-Source Medium-High-Resolution Remote Sensing Data of China," *Remote Sens. Vol. 14*, 5590, 2022
2. Kabir, S., L. Leigh, L., and D, Helder, "Vicarious Methodologies to Assess and Improve the Quality of the Optical Remote Sensing Images: A Critical Review," *Remote Sens.* vol. *12*, 4029, 2020
3. Claverie, M., J. Ju,, J.G. Masek, J.L. Dungan, E.F. Vermote, J.C. Roger, S.V. Skakun, and C. Justice, "The Harmonized Landsat and Sentinel-2 *S*urface *R*eflectance *D*ata *S*et," *Remote Sens. Environ* vol. 219, 2018.
4. NASA, MODIS, Moderate Resolution Imaging Spectroradiometer. Available online: https://modis.gsfc.nasa.gov/ (accessed 3-13-2023), undated
5. Planet Labs. Planet Fusion Monitoring Technical Specification Version 1.0.0. 2022. Available online: https://assets.planet.com/docs/Fusion-Tech-Spec_v1.0.0.pdf (accessed on 1-7-2023).
6. USGS. Undated. Landsat 8 data users handbook. https://www.usgs.gov/landsat-missions/landsat-8-data-users-handbook, (accessed 5-30-2023).
7. Groeneveld, D.P., T.A. Ruggles, and B-C Gao, "Closed-Form Method for Atmospheric Correction (CMAC) of Smallsat Data Using Scene Statistics. *Appl. Sci.* vol.13, 6352, 2023.
8. Vermote, E., *J.C.* Roger, B. Franch, and S. Skakun, "LaSRC (Land Surface Reflectance Code): Overview, application and validation using MODIS, VIIRS, LANDSAT and Sentinel 2 data," In Proceedings of the IGARSS 2018—2018 IEEE International Geoscience and Remote Sensing Symposium, *2018*.
9. Guidi, L. M. Tattini, and M. Landi, "How Does Chloroplast Protect Chlorophyll Against Excessive Light? *Intech*. DOI:10.5772/67887, 2017.
10. Kume, A. Importance of the green color, absorption gradient, and spectral absorption of chloroplasts for the radiative energy balance of leaves. *J. Plant Res.* Vol. *130*, 2017.
11. Karpouzli, E. and T. Malthus, "The empirical line method for the atmospheric correction of IKONOS imagery. *Int. J. Remote Sens* Vol. 24, 2003.
12. Fraser, R.S.; Kaufman, Y.J. "The relative importance of aerosol scattering and absorption in remote sensing.," *IEEE Trans Geosci. Remote Sens.*,Vol. *GE-23*, 1985.
13. Richter, R.; Louis, J.; Muller-Wilm, U. Sentinel-2 MSI-Level 2A Products Algorithm Theoretical Basis Document, S2PAD-ATBD-0001, 2012.
14. Baugh, W. and D.P. Groeneveld, "Empirical proof of the empirical line," *Int. J, Rem. Sen.* Vol. 9., 2008.
15. Groeneveld, D.P. and D.D. Barz, Remote monitoring of surfaces wetted for dust control on the dry Owens Lakebed, California. *Open J. Mod. Hydrol.* Vol. 3, 2013.

Acknowledgements: The research to create CMAC was supported by the US National Science Federation Small Business Innovation Research program. This research could not have been completed without the quality, cadence and resolution of data from the Sentinel 2 program

APPENDIX A.

Statistics provided an opportunity to evaluate the performance of the software packages CMAC, Sen2Cor and LaSRC for surface reflectance retrievals. However, they represent a limited abstraction of the information from the image corrections. Appendix A provides representative scenes from S2 and L8 images as a synoptic view of the surface reflectance retrievals. Earlier efforts verified that atmospherically corrected images that display correct color balance with haze removed provide close approximations of surface reflectance [7].

The following pages present S2 and L8/9 images in four versions that are presented from top to bottom: TOAR, Atm-I grayscale, CMAC and the corrected images from the Sen2Cor and LaSRC packages, respectively, Sen2Cor for Sentinel 2 data and LaSRC for Landsat 8/9.

The views produced for Appendix A are the output from CMAC, Sen2Cor and LaSRC with no additional processing except for minor adjustments of image stretch by one or two percent to brighten their appearance. As a reference for understanding Atm-I, images taken through unusually clean atmospheres have Atm-I generally below ~825.

In all such image-to-image visual comparisons to LaSRC and Sen2Cor including those presented here, CMAC images are generally clearer and exhibit better overall color balance.

S2, Coast north of Veracruz, MX 5-03-2021
1200 to 1300 Atm-I

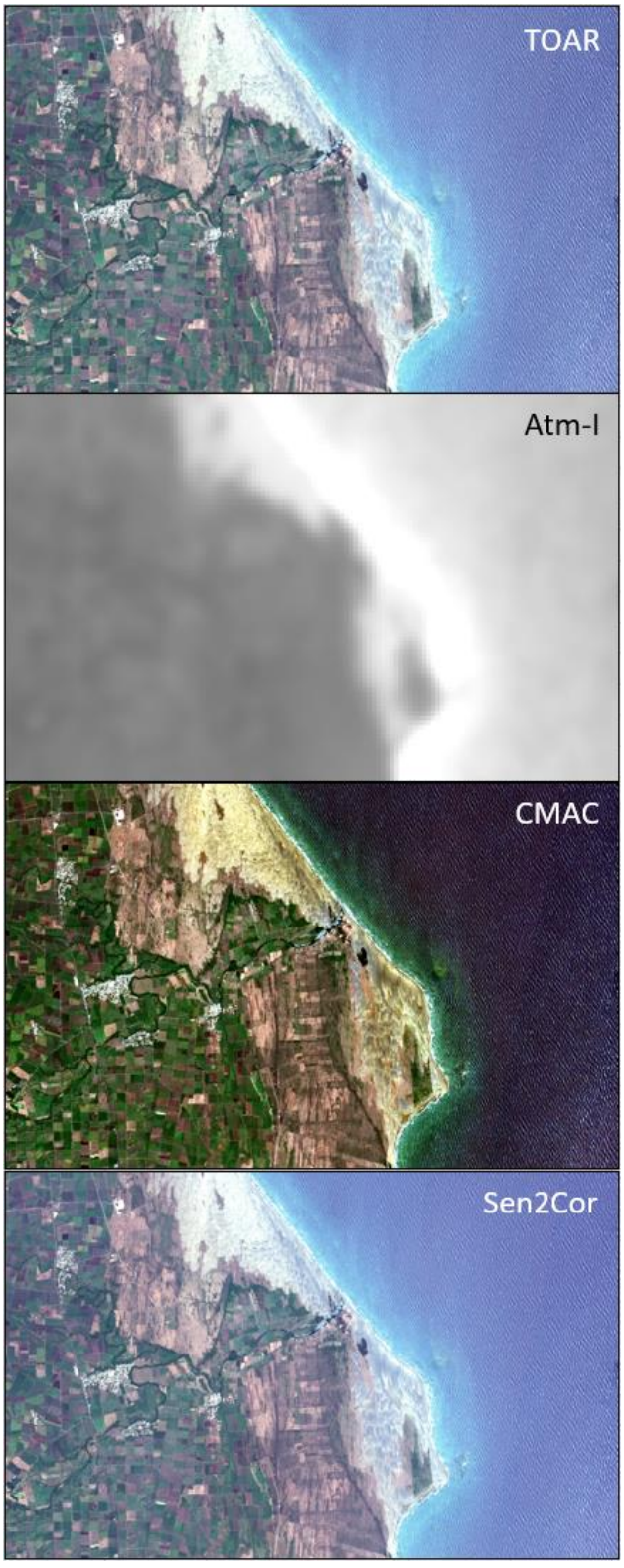

S2, Gillette, WY and regional coal mines 7-25-2021
1125 to 1225 Atm-I

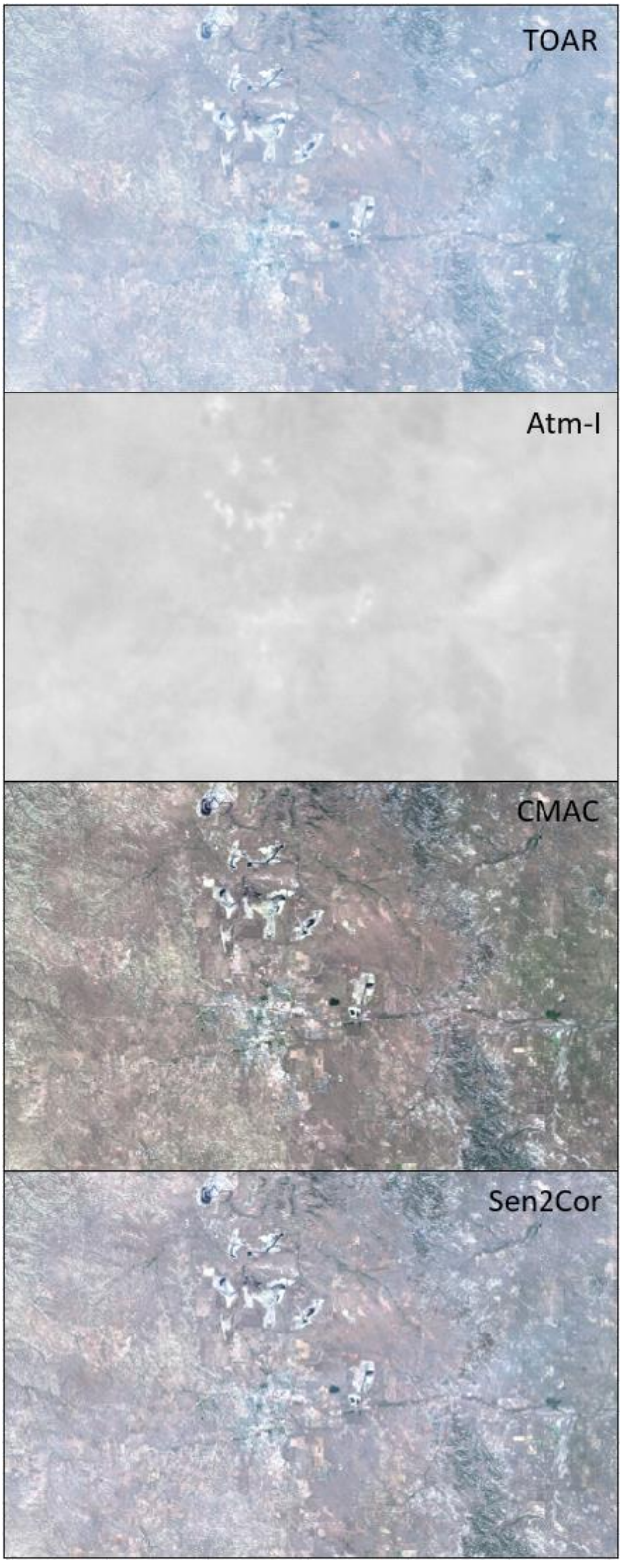

S2, Slave Lake, Alberta, CA 5-14-2023
880 to 1490 Atm-I

S2, near Alexandria, Minnesota, US 5-16-2023
1140 to 1250 Atm-I

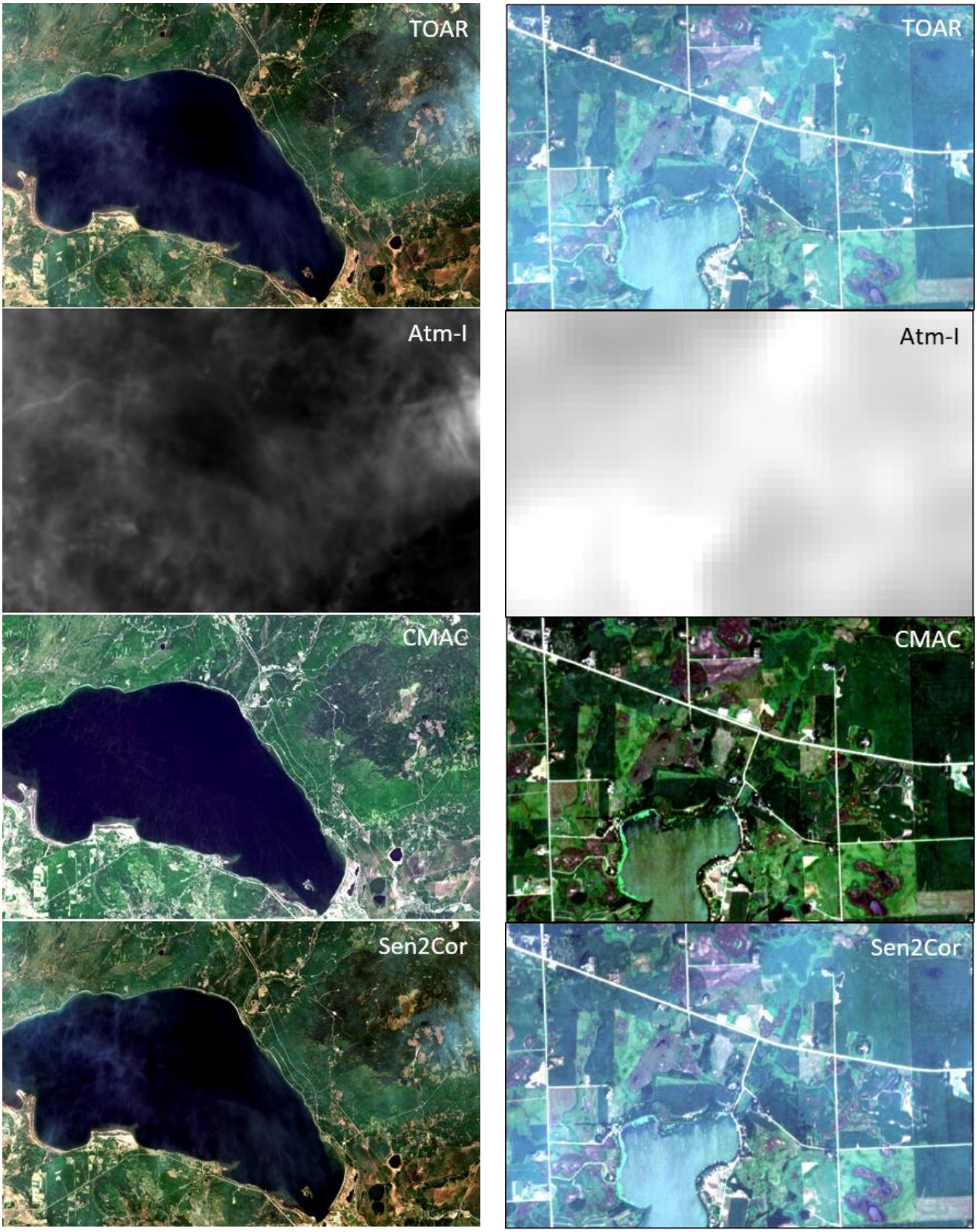

S2, near Athabasca, Alberta, CA, 5-16-23
850 to 1700 Atm-I

S2, Chiang Mai, Thailand, 2-13-21
790 to 1100 Atm-I

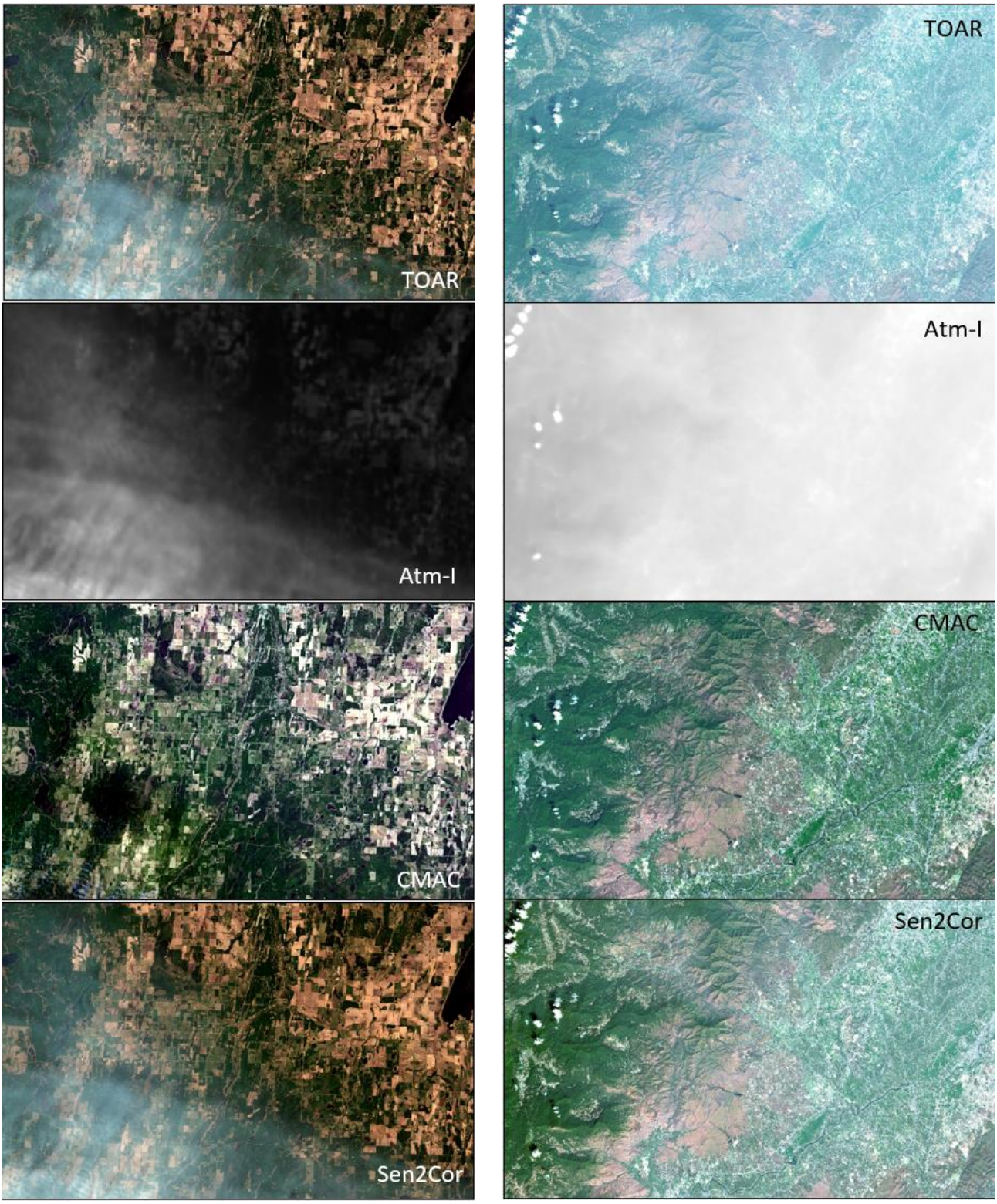

L8, Kamloops, British Columbia, CA 8-3-2021
885 to 1430 Atm-I

L8, Near Lethbridge, Alberta, CA 7-31-2021
1275 to 1540 Atm-I

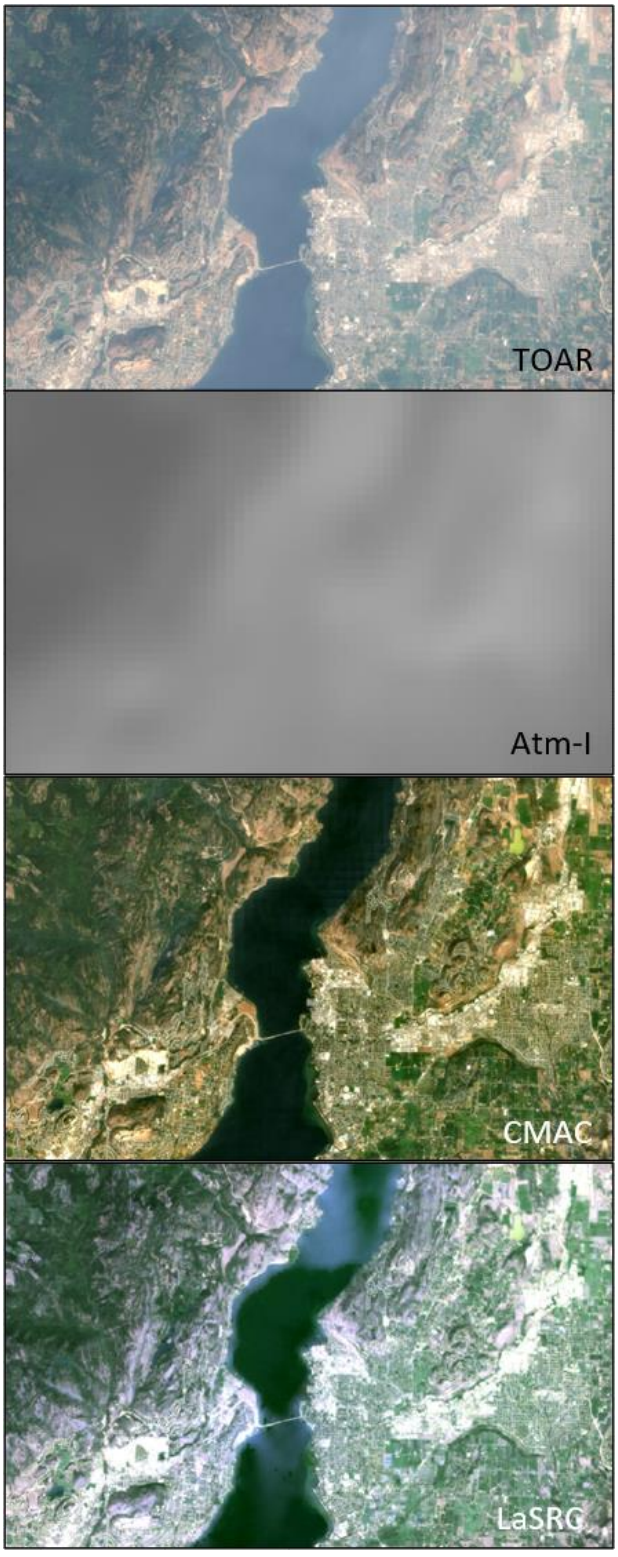

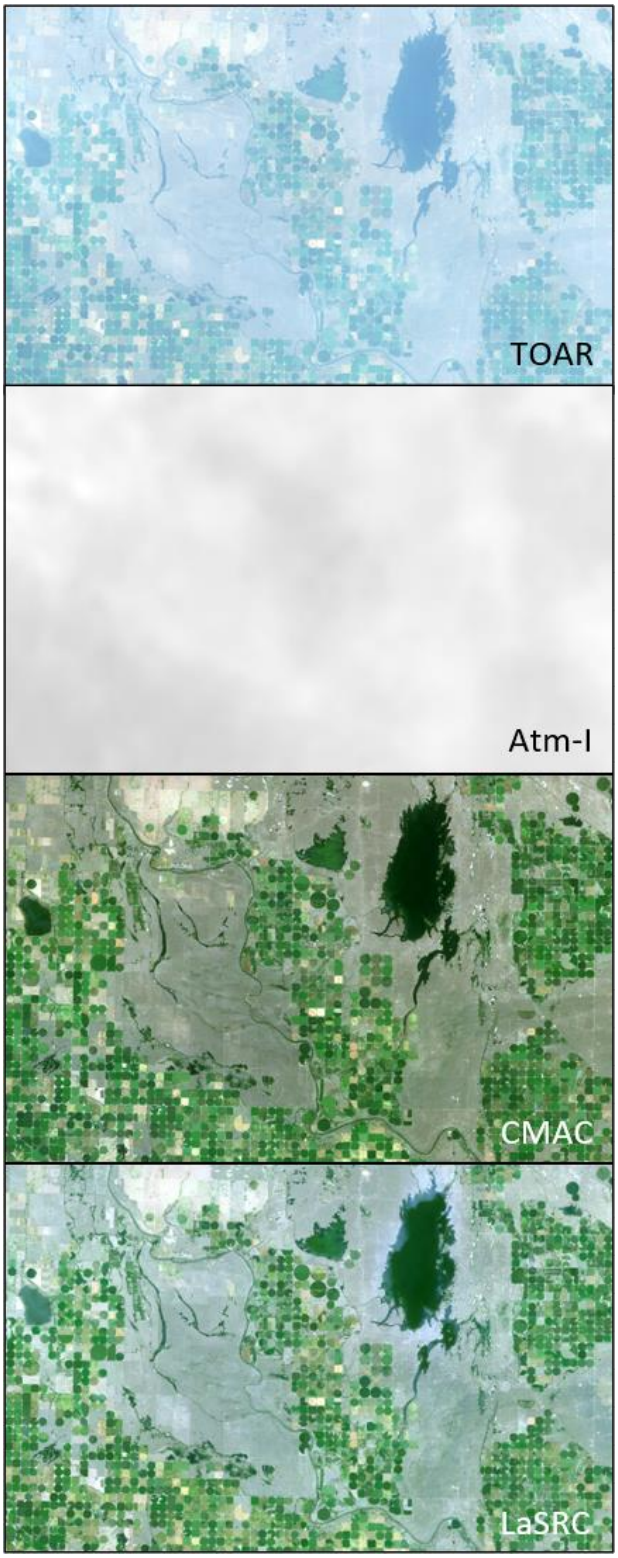

L8, Kindersley, Saskatchewan, CA 8-03-2021
885-1430 Atm-I

L8, Near Alexandria, Minnesota, US 7-11-2021
1150 to 1335 Atm-I

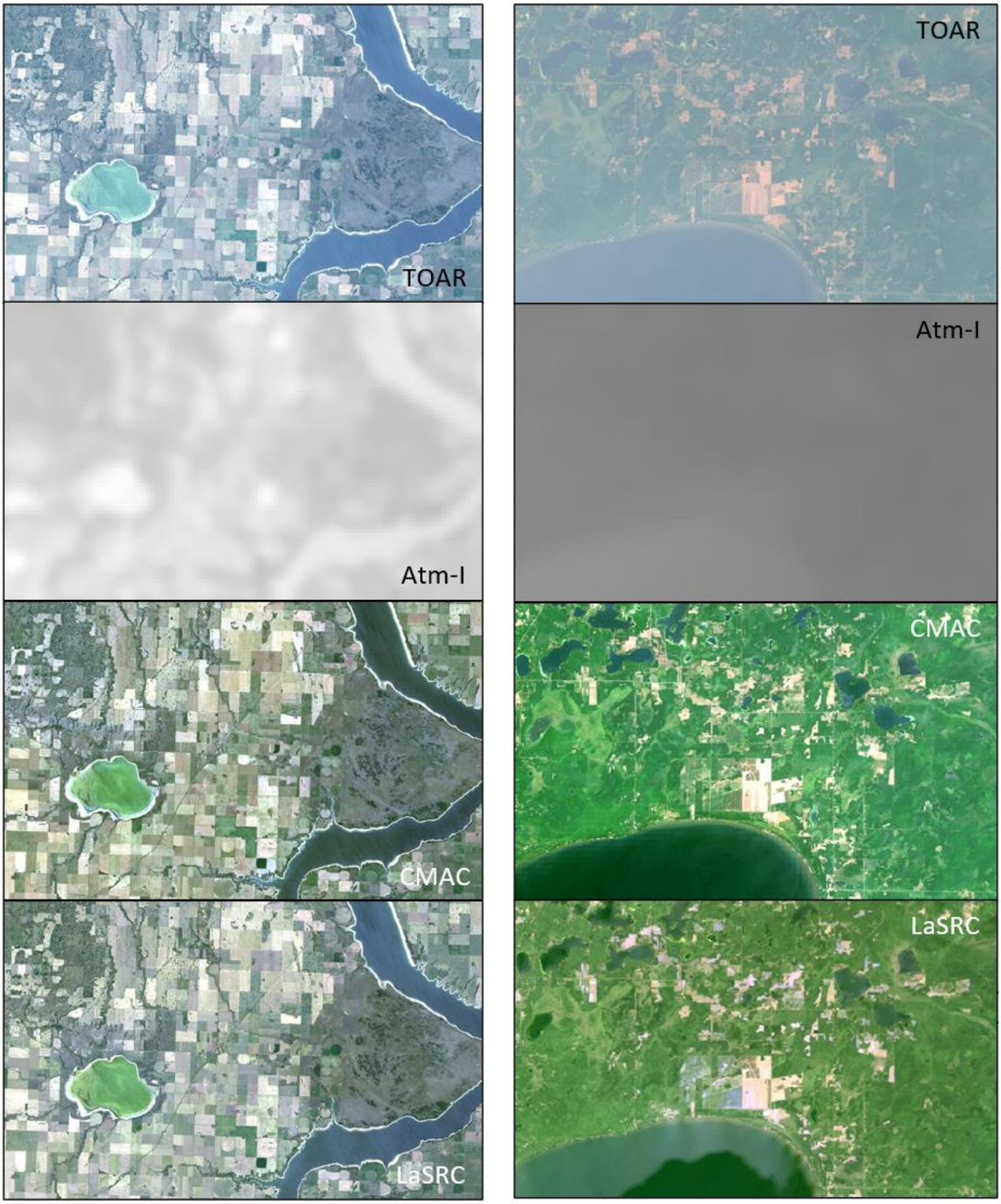

L8, Halifax, Nova Scotia, CA 7-11-2021
1150-1335 Atm-I

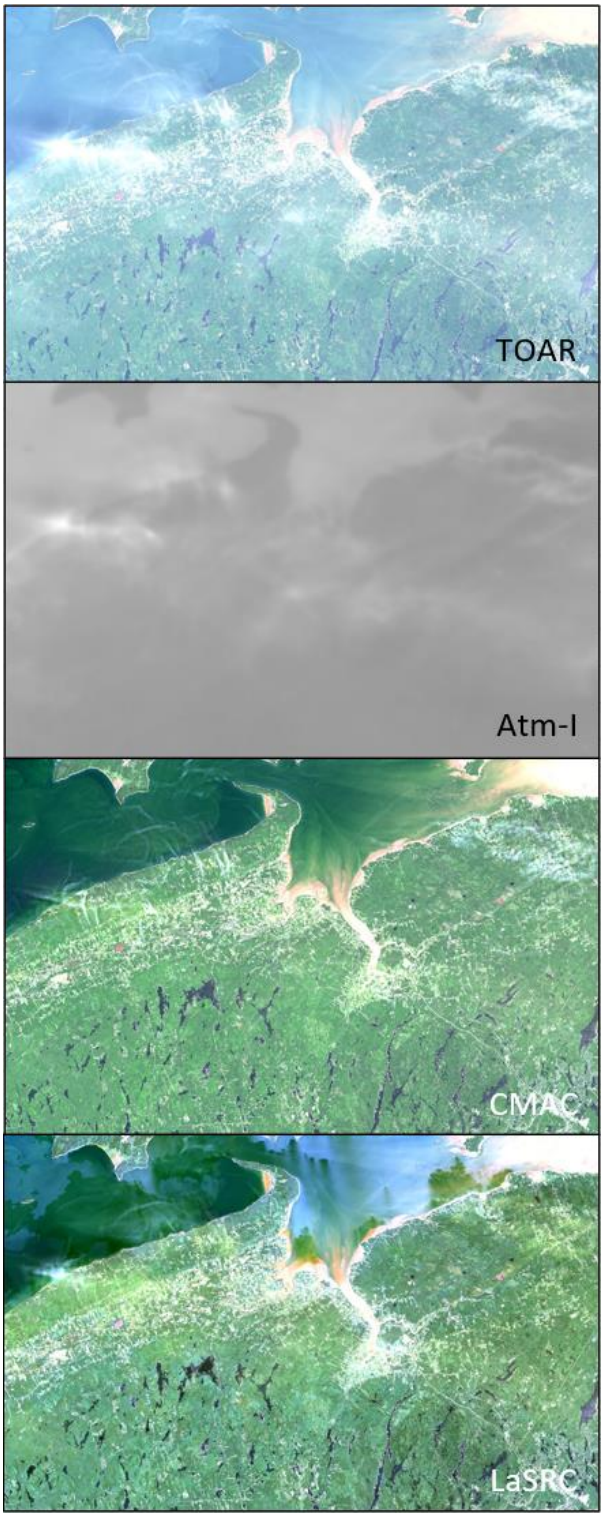

L8, Cape Hatteras, North Carolina, US 7-25-2021
820 to 1300 Atm-I

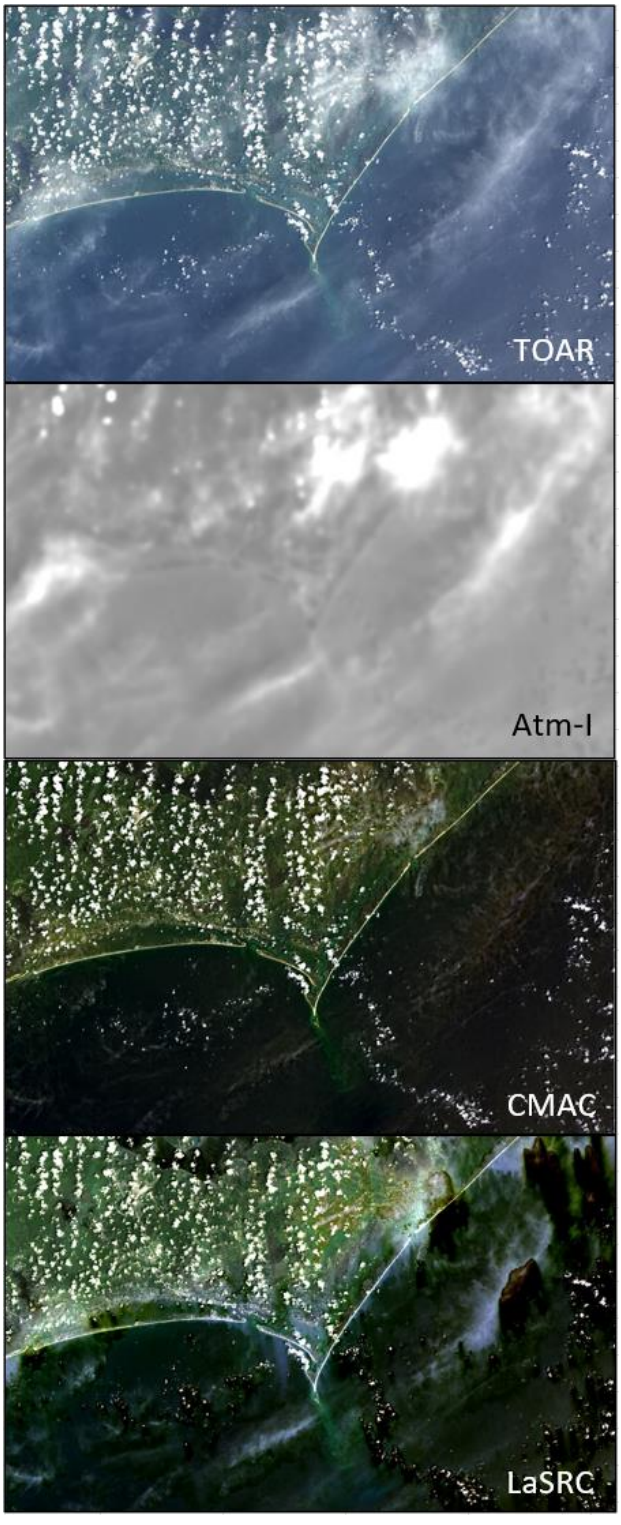

Preliminary (proof of concept) master-proxy calibrated test corrections of Planet Dove cubesat images of North and South Dakota and Northern California Coast. Atm-I levels varied from about 900 to 1050. Other than the calibration, no other adjustment is needed for smallsats.